Ultrafast conductivity in a low-band-gap polyphenylene and fullerene blend studied by terahertz spectroscopy

Hynek Němec,[1,2] Han-Kwang Nienhuys,[3] Erik Perzon,[4] Fengling Zhang,[5] Olle Inganäs,[5] Petr Kužel,[2] and Villy Sundström[1]
[1]*Department of Chemical Physics, Lund University, Getingevägen 60, 222 41 Lund, Sweden*
[2]*Institute of Physics, Academy of Sciences of the Czech Republic, 182 21 Prague, Czech Republic*
[3]*FOM Institute for Atomic and Molecular Physics, Kruislaan 407, 1098SJ Amsterdam, The Netherlands*
[4]*Department of Chemical and Biological Engineering, Chalmers University, 412 96 Göteborg, Sweden*
[5]*Biomolecular and Organic Electronics, IFM, Linköping University, 581 53 Linköping, Sweden*
(Received 6 April 2009; published 24 June 2009)

Time-resolved terahertz spectroscopy and Monte Carlo simulations of charge-carrier motion are used to investigate photoinduced transient conductivity in a blend of a low-band-gap polyphenylene copolymer and fullerene derivative. The optical excitation pulse generates free holes delocalized on polymer chains. We show that these holes exhibit a very high initial mobility as their initial excess energy facilitates their transport over defects (potential barriers) on polymer chains. The conductivity then drops down rapidly within 1 ps, and we demonstrate that this decrease occurs essentially by two mechanisms. First, the carriers loose their excess energy and they thus become progressively localized between the on-chain potential barriers—this results in a mobility decay with a rate of $(180\ \mathrm{fs})^{-1}$. Second, carriers are trapped at defects (potential wells) with a capture rate of $(860\ \mathrm{fs})^{-1}$. At longer time scales, populations of mobile and trapped holes reach a quasiequilibrium state and further conductivity decrease becomes very slow.

DOI: 10.1103/PhysRevB.79.245326 PACS number(s): 78.47.J−, 72.20.Jv, 72.80.Le, 78.66.Qn

I. INTRODUCTION

Materials based on conjugated organic semiconductors are extensively explored in view of promising application, for instance, in inexpensive solar cells.[1] Development of efficient materials requires detailed understanding of the fundamental photoinitiated processes in these systems. The primary excitation in polymer/fullerene bulk heterojunctions is an exciton on the polymer chain, which dissociates within tens of fs: the electron is transferred to the fullerene ball while the hole remains on the polymer chain.[2,3] Initially, the holes move along the chain on which they were generated. The hole interchain transport is much slower, nevertheless, it is a prerequisite for collection of charges on electrodes.

It has been speculated that photogenerated charges are initially very mobile and that they quickly loose their mobility due to the potential-energy landscape of conjugated polymers controlled by the disorder.[4] However, the nature of the early stages of the intrachain transport remains unclear, namely, due to the lack of tools able to probe the local transport properties with subpicosecond time resolution at low probing fields. All-optical pump-probe methods offer an excellent time resolution, but they are insensitive to the transport.[3,5] The transport mechanisms can be studied using time-of-flight or time-resolved microwave conductivity techniques; however, the time resolution is usually not better than nanoseconds.[6–8] Subpicosecond time resolution and sensitivity to the transport properties in transient Stark spectroscopy is paid by the necessity to apply very high electric fields (MV/cm) which often fundamentally affect the mobility.[9] A technique of choice is then time-resolved terahertz (THz) spectroscopy[10,11] which offers subpicosecond time resolution and uses low probing fields (kV/cm). The method is highly sensitive to the degree of localization of charge carriers[12] and it directly yields their far-infrared conductivity which contains information about the carrier density and the carrier local mobility.

So far, mainly conventional polymers [such as poly(2-methoxy-5-(2′-ethyl-hexyloxy)-*p*-phenylene-vinylene) (MEH-PPV) or poly(3-hexylthiophene) (P3HT)] and their blends with fullerene derivative [(6,6)-phenyl-C_{61}-butyric acid methyl ester (PCBM)] were studied by time-resolved THz spectroscopy and the investigations focused on times ≥ 1 ps. The interpretation of transient conductivity spectra in these materials still remains a subject of discussion. A microscopic picture proposed by Hendry *et al.*[13–15] is based on calculations of the mobility in a tight-binding approximation which reflects the effects of torsional disorder on infinite polymer chains.[16] However, matching of the calculated and measured THz conductivities required a nontrivial extrapolation of microwave conductivity values[15] in order to account for the mobility reduction due to the chain termination, conjugation defects, and energetic disorder. Other groups[17–19] describe the response of carriers using the purely phenomenological Drude-Smith model[20] which does not bring a new insight into the microscopic origin of the transient response.[12]

In our former work on a low-band-gap polyfluorene copolymer and its blend with PCBM, we tried to interpret the transient subnanosecond response in terms of dielectric relaxations with two distinct relaxation times.[21] In this paper, we achieve a time resolution of ~200 fs and develop a microscopic model of conductivity showing that these relaxations correspond to the intrachain motion of carriers over two distinct length scales delimited by potential barriers on polymer chains and by the chain terminations. We show that the carriers are initially mobile: they have a certain excess energy which allows them to pass easily over the potential barriers. As the carriers cool, the barriers progressively start to limit their motion. The ultrafast response we observe can

be envisaged for a design of ultrafast switches based on organic materials. The quantitative information about the potential barriers may provide helpful hints for optimizing the film morphology aimed at obtaining much better macroscopic mobility.

II. EXPERIMENTAL

The investigated polymer LBPP-1 consists of an alternating sequence of two types of monomer units: a low band-gap segment and a dialkoxy-phenylene unit. The low band-gap segment contains a central electron accepting 2-thia-1,3,5,8-tetraaza-cyclopenta[b]naphthalene unit bordered by electron donating thiophene units on each side.[22] This copolymer was dissolved in chloroform and blended with the soluble fullerene derivative PCBM in a weight ratio 1:4 (polymer:PCBM). An approximately 1-μm-thick film was prepared by drop casting the solution on a fused silica substrate. Unlike most conventional polymers, LBPP-1 exhibits an additional near-infrared absorption band extending to more than 1100 nm.

The transient THz conductivity was measured in usual setups for optical pump-THz probe experiments.[23] The sample was excited by ultrashort optical pulses at 800 nm or 620 nm at excitation densities $7-9\times10^{19}$ cm^{-3}. The key output of these experiments was the transient THz waveform (photoinduced change in the THz pulse transmitted through the sample) $\Delta E(\tau,\tau_p)$ measured as a function of time τ and of the pump-probe delay τ_p. Depending on the investigated time scales, the retrieval of transient conductivity $\Delta\sigma$ from these data then requires different approaches.

For dynamics slower than the THz probe pulse length, the state of the sample does not change during the probing event and the quasi-steady-state approximation applies. The spectral information about the investigated dynamics is contained in the time-dependent transient conductivity spectrum $\Delta\sigma(f,\tau_p)$ (f is the probing THz frequency) which is directly proportional to the photoinduced change $\Delta E(f,\tau_p)$; the proportionality function depends on the ground-state properties of the sample, and it can be determined easily.[23,24] In this regime, it is sufficient to measure the conductivity spectra for several representative pump-probe delays. We also checked the conductivity behavior with attenuated excitation beam intensity.

For short pump-probe delays and for dynamics faster or comparable to the THz probe pulse length, it is essential to treat correctly the frequency mixing due to the ultrafast evolution of the sample properties.[25,26] Here we employ the analysis in the two-dimensional (2D) frequency space (f,f_p) which shows that the transient conductivity $\Delta\sigma(f,f_p)$ is directly proportional to $\Delta E(f,f_p)$ in the 2D frequency space.[24,26] The frequency f is conjugated to the delay τ, and it denotes the spectral components of the transmitted THz pulse, while the frequency f_p is conjugated to the delay τ_p and it is related to the dynamical evolution of the system. The measurement and its analysis closely followed the procedures described in Refs. 23 and 27 and a few further technical details are discussed in Appendix A. The transient THz waveforms at subpicosecond times were measured in a carefully aligned collinear pump-probe arrangement on a uniform grid of 82×76 points separated by 80 fs steps in both directions $(\tau\times\tau_p)$, providing data in a rectangle with dimensions 6.56×6.08 ps^2. The pump-probe delay was varied from $\tau_{p,\min}$ (<0 ps) to $\tau_{p,\max}$, where the time origin (0 ps) represents the temporal overlap of the pump and probe pulses. Note that due to the large amount of data collected in this experimental regime, it was not possible to investigate the dependence of the ultrafast transient conductivity on the excitation fluence. The setup for the ultrafast conductivity measurements was available for the 800 nm excitation only.

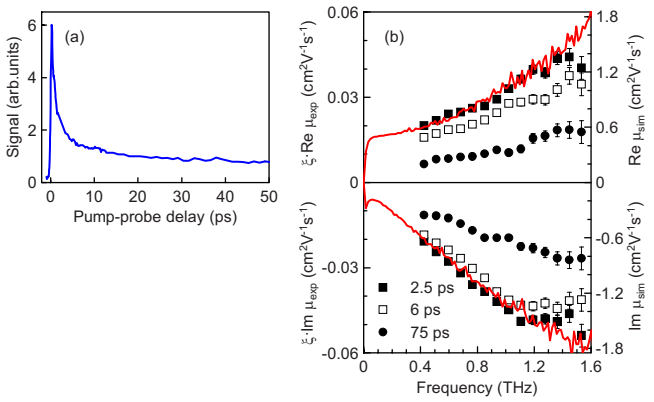

FIG. 1. (Color online) (a) Pump-probe scan measured without spectral resolution. (b) Measured spectrum of yield-mobility product at three representative pump-probe delays (symbols, left axis) and mobility obtained in the Monte Carlo calculations (lines, right axis). Excitation wavelength was 620 nm in both graphs.

III. RESULTS AND DISCUSSION

A pump-probe scan without the spectral resolution, expressing the time dependence of the photoconductivity of the studied system, is shown in Fig. 1(a). It displays an instantaneous activation followed by a subpicosecond decay. The decay then slows down considerably so that a nonvanishing signal is observed even 1 ns after photoexcitation. These two regimes will be addressed separately in the following two sections as they need to employ the two different methods for the conductivity analysis described above.

We suppose that the observed transient conductivity is dominated by the response of holes on polymer chains. The measured response cannot originate from the response of electrons accepted by the PCBM: their mobility characterized by transient Stark spectroscopy[9] is considerably lower than mobilities observed in the blend and presented later on. The large gap of PCBM also prevents its direct excitation due to the long excitation wavelengths employed in the experiments.

A. Slow conductivity component

Examples of transient conductivity spectra for a few pump-probe delays measured with the 620 nm excitation are shown in Fig. 1(b). The observed spectrum (increasing real part and negative imaginary part) is characteristic for the response of localized charge carriers. We fit the spectra by a

sum of two Debye relaxations[28] (later we demonstrate that the two relaxations have their counterparts in the subpicosecond spectra and that the first relaxation is due to the finite polymer chain length and the second one arises from the potential barriers on the chains):

$$\Delta\sigma(f,\tau_p) = n_0 e_0 \xi(\tau_p) \underbrace{\sum_{j=1}^{2} \mu_j \frac{2\pi i f \theta_j}{2\pi i f \theta_j - 1}}_{\mu(f)}, \tag{1}$$

where n_0 is the number of absorbed pump photons per unit volume, e_0 is the elementary charge, μ_j is the high-frequency mobility of the jth relaxation, and θ_j is its relaxation time. The term $n_0\xi(\tau_p)$ expresses the density of mobile charge carriers and $\mu(f)$ is their mobility spectrum. The quantity $\xi(\tau_p)$ thus identifies the (instantaneous) density of mobile charge carriers normalized by the excitation density—for the sake of simplicity, we will call this quantity a yield of carriers. Note that in Eq. (1), ξ may decrease due to both carrier capture and recombination and μ is the mobility of mobile—noncaptured—carriers.

The shape of the experimental spectra does not change significantly with τ_p. Their fit by Eq. (1) yields time-independent relaxation times $\theta_1=60$ fs and $\theta_2 \gtrsim 10$ ps and the conductivity amplitudes, e.g., at $\tau_p=2.5$ ps we find $\xi\mu_1 = 0.12$ cm^2 V^{-1} s^{-1} and $\xi\mu_2=0.016$ cm^2 V^{-1} s^{-1}. Fitting parameters of the spectra measured with 800 nm excitation differ by less than 20%.

A single Debye relaxation appeared as the leading term in the expression for the mobility derived by Prins *et al.*,[29] where the transport mechanism was the carrier diffusion limited by infinite barriers representing chain ends. Inspection of Eq. (6) in Ref. 29 allows one to deduce the corresponding relaxation time

$$\theta = \frac{e_0 (Na/\pi)^2}{\mu_{\text{int}} k_B T}, \tag{2}$$

where N is the number of repeat units enclosed with the barriers, a is the repeat unit length ($\approx$1.5 nm for LBPP-1), μ_{int} is the intrinsic mobility (intrachain mobility along infinite polymer chains without defects), k_B is the Boltzmann constant, and T is temperature.

Below we extend the Prins' model of mobility by considering potential barriers or potential wells on the polymer chain. We show that the two observed relaxation terms from Eq. (1) can be accounted for when the polymer chains contain *finite* potential barriers, while the presence of potential wells influences mainly the mobility amplitude, not its spectrum.

In the Monte Carlo calculations we consider straight polymer chains consisting of N equidistantly spaced repeat units and terminated by perfectly reflecting (infinite) potential barriers. The holes can hop between the nearest-neighboring unit and the mean time for the hop to a given neighbor is $\tau_{\text{hop}}=a/v$. Later we prove that τ_{hop} is very short which can be achieved by taking the mean velocity v as the thermal velocity $\sqrt{k_B T/m}$ (with the hole effective mass m equal to the mass of a free electron we get $\tau_{\text{hop}} \approx 22$ fs)—in this case the transport is very fast and its bandlike character cannot be excluded.

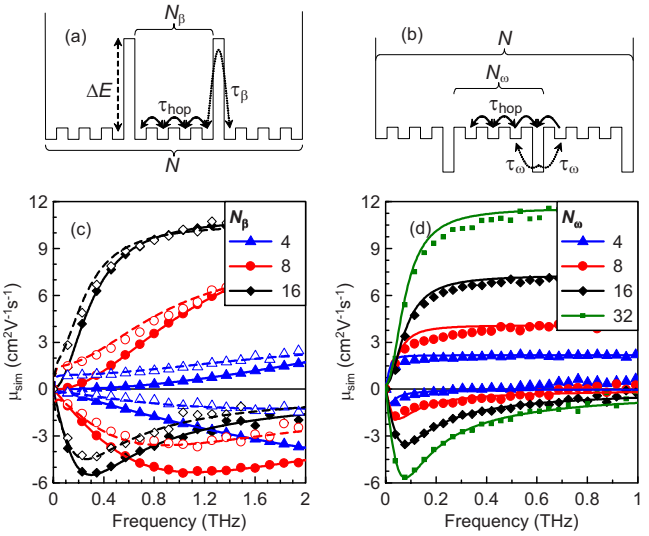

	$\tau_\beta = \infty$		$\tau_\beta = 50\tau_{hop}$	
N_β	θ_1 (ps)	θ_2 (ps)	θ_1 (ps)	θ_2 (ps)
16	0.53	—	0.60	16
8	0.14	—	0.16	16
4	0.037	—	0.085	13

N_ω	θ_1 (ps)
32	2.0
16	2.0
8	3.2
4	3.5

FIG. 2. (Color online) Upper row: sketch of the potential profile used in the simulations of mobility on polymer chains with (a) potential barriers and (b) potential wells. (c) Calculated mobility spectra of holes moving on polymer chains with infinite ($\tau_\beta=\infty$, closed symbols) and finite barriers ($\tau_\beta=50\tau_{\text{hop}}$, open symbols) and for several numbers N_β of repeat units enclosed between the barriers (the polymer chain always contained $N=32$ repeat units in total). Solid lines: fits of spectra calculated for the infinite barriers by a single relaxation term: dashed lines: fits of spectra calculated for the finite barriers by two relaxation terms. (d) Symbols: calculated mobility spectra of holes moving on polymer chains with variable density of potential wells ($N=32$ and $\tau_\omega=20\tau_{\text{hop}}$). Lines show the fits by a single relaxation term. Bottom row: relaxation times obtained from fits of the calculated spectra by one or two relaxation terms.

Further on, we introduce two types of defects on the polymer chains. First, we investigate the influence of potential barriers enclosing segments of N_β repeat units [Fig. 2(a)]. The mean time for passing over the barrier is then denoted τ_β. Infinite barriers are characterized by $\tau_\beta=\infty$, while the absence of barriers can be mimicked by setting $\tau_\beta=\tau_{\text{hop}}$. Second, we study the response of chains containing potential wells (traps) placed regularly at each N_ωth repeat unit [Fig. 2(b)]. In this case, the mean release time is $\tau_\omega/2$ and absence of traps is represented by the value of $\tau_\omega=\tau_{\text{hop}}$. A Monte Carlo simulation is used to find trajectories of individual carriers. The mobility spectrum $\mu(f)$ is calculated using the modified Kubo formula[30] in which the averaging takes place over a canonical ensemble of carriers and over all orientations of straight polymer chains. We also define an intrinsic on-chain mobility of oriented infinite chains without defects ($N\to\infty$). In this limit, the diffusion coefficient equals a^2/τ_{hop} and the Einstein's relation then provides the mobility

$$\mu_{\text{int}} = \frac{e_0 a^2}{k_B T \tau_{\text{hop}}}. \quad (3)$$

A similar simulation considering either the barriers or the traps has been employed in Ref. 31 for the calculation of time dependence of the diffusion coefficient and mobility along polymer chains containing a Gaussian distribution of energies of barrier heights or trap depths. In our work, we concentrate on the calculations of the mobility spectra at THz frequencies. Furthermore, we set the height of the barriers or the depth of the traps to one given value. On the one hand, taking a realistic distribution of barrier heights or trap depths would be more adequate for comparison with experimental data. On the other hand, the employment of the delta distribution provides a clear picture of influence of defects on polymer on the THz mobility spectra.

In Fig. 2(c), we illustrate the mobility spectra for carriers moving along chains containing infinite and finite potential barriers. When the barriers are infinite ($\tau_\beta \to \infty$), the spectrum can be accounted for by a single relaxation term. Its relaxation time θ_1 is very short for short-segment lengths and it increases with N_β: by inspection of Eqs. (2) and (3), we can derive $\theta_1 \approx \tau_{\text{hop}}(N_\beta/\pi)^2$ which is confirmed by the simulations. The high-frequency mobility approaches one third of the intrinsic mobility μ_{int}—the factor of 1/3 accounts for the random orientations of polymer chains. Lowering the barriers (i.e., making τ_β finite) results in the growth of the low-frequency mobility; the second relaxation with a long relaxation time θ_2 is then required to fit the calculated spectra. The short and long relaxation times correspond to the diffusion times along the segments and the entire chain, respectively. Since N_β must be greater or equal to 2, it turns out that θ_1 cannot be shorter than $\tau_{\text{hop}} \cdot (2/\pi)^2$—in other words, the value of θ_1 imposes the upper limit on the value of the hopping time τ_{hop}.

The influence of potential wells is shown in Fig. 2(d). Regardless the density of traps and τ_ω, the spectra are always described essentially by a single relaxation term. The most remarkable change with increasing density of potential wells (i.e., with decreasing N_ω) is a decrease in the mobility amplitude while only a slight increase in the relaxation time is observed. These findings allow us to assume for simplicity that a part of the carriers [$n_0\xi$ in terms of Eq. (1)] moves along the chains without traps and the time decrease in the yield $\xi(\tau_{\text{p}})$ describes the carrier trapping into states not contributing the THz conductivity. A given value of ξ can be achieved by various combinations of τ_ω and N_ω and it is not possible to determine unambiguously, e.g., the density of traps N/N_ω.

Since the measured spectra are represented by two relaxation terms and not by a single one, the model above indicates the existence of potential barriers within the LBPP-1 chains. The spectra are dominated by the relaxation with the short relaxation time (θ_1). The small value of θ_1 found experimentally evidences that the distance between the barriers (N_β) is small and the intrasegment transport is short range. It also justifies the estimate of τ_{hop} entering the simulations and shows that the intrinsic carrier mobility along (nondefective) LBPP-1 chains is high: $\mu_{\text{int}} \sim 40$ cm^2 V^{-1} s^{-1}. The relaxation with the long relaxation time (θ_2) expresses the intersegment transport. Its low amplitude indicates that the barriers between the segments are rather high. The experimental data can be matched with $N_\beta = 4$ and $\tau_\beta = 1.9$ ps [Fig. 1(b)]. No drop in the real part of the mobility spectra is observed at low frequencies. This is possible only for long relaxation time: we estimate that $\theta_2 \gtrsim 10$ ps. The simulations confirm that this occurs for chains containing $\gtrsim 26$ repeat units, which is consistent with the number average of repeat units per chain x_n of LBPP-1.[22] We can further assume that the jumps over the barriers are thermally activated, i.e., $\tau_\beta = \tau_{\text{hop}} e^{\Delta E/(k_B T)}$ which provides an estimate of the barrier height $\Delta E \sim 120$ meV.

The large difference between the simulated mobility and the measured yield-mobility product [Fig. 1(b)] demonstrates that the majority of carriers is trapped and does not contribute to the conductivity. This means that either there is a high density of shallow potential wells (with short τ_ω) or that there is a lower density of deep potential wells (long τ_ω). Note also that we did not observe any nonlinear phenomena at the excitation densities employed: decreasing the excitation fluence by a factor of 10 led to a tenfold decrease in the conductivity without a significant change in the shape of the conductivity spectrum.

In Ref. 21 we speculated that a part of the response may be due to bound polaron pairs. However, the presented simulations show that the observed response arises from a fast motion over rather long distances ($\approx aN_\beta$), which means that the observed conductivity must be mediated by separated charge carriers.

It should be also noted that the defects on real polymer chains always show some distribution. In this respect, the particular value of $N_\beta = 4$ found by the simulations mainly indicates that there is a high density of potential barriers. These may appear due to conjugation defects or torsional disorder.[16] We have also shown that the influence of the density of traps and their occupation can be fully encoded into the evolution of $\xi(\tau_p)$. However, this is only true for the conductivity spectra in the THz range which are sensitive mainly to the most mobile carriers. In contrast, accounting for the distribution of release times and of the occupancy of the trap levels is essential in calculating low-frequency conductivity which is determined by all (not only the most mobile) charge carriers.[8]

With the help of the Monte Carlo simulations we proposed microscopic mechanisms on which our conductivity model is built. It is possible to devise several ways of its validation. The temperature of carriers—regardless their initial energy—should be close to the temperature of the polymer backbone for long pump-probe delays. This means that in the first approximation, the mobility spectrum should be independent of the excitation wavelength. In the present work, no significant difference in mobilities was observed for photoexcitation at 800 and 620 nm. Transient conductivity spectra practically independent of the excitation wavelength were also observed in P3HT.[18,19] Measurements of the temperature dependence then should provide an independent validation of the transport model employed. Assuming that the passage over the barriers is a thermally activated process, decreasing the temperature should dramatically lengthen the time τ_β. This would result in a decrease in the amplitude μ_2

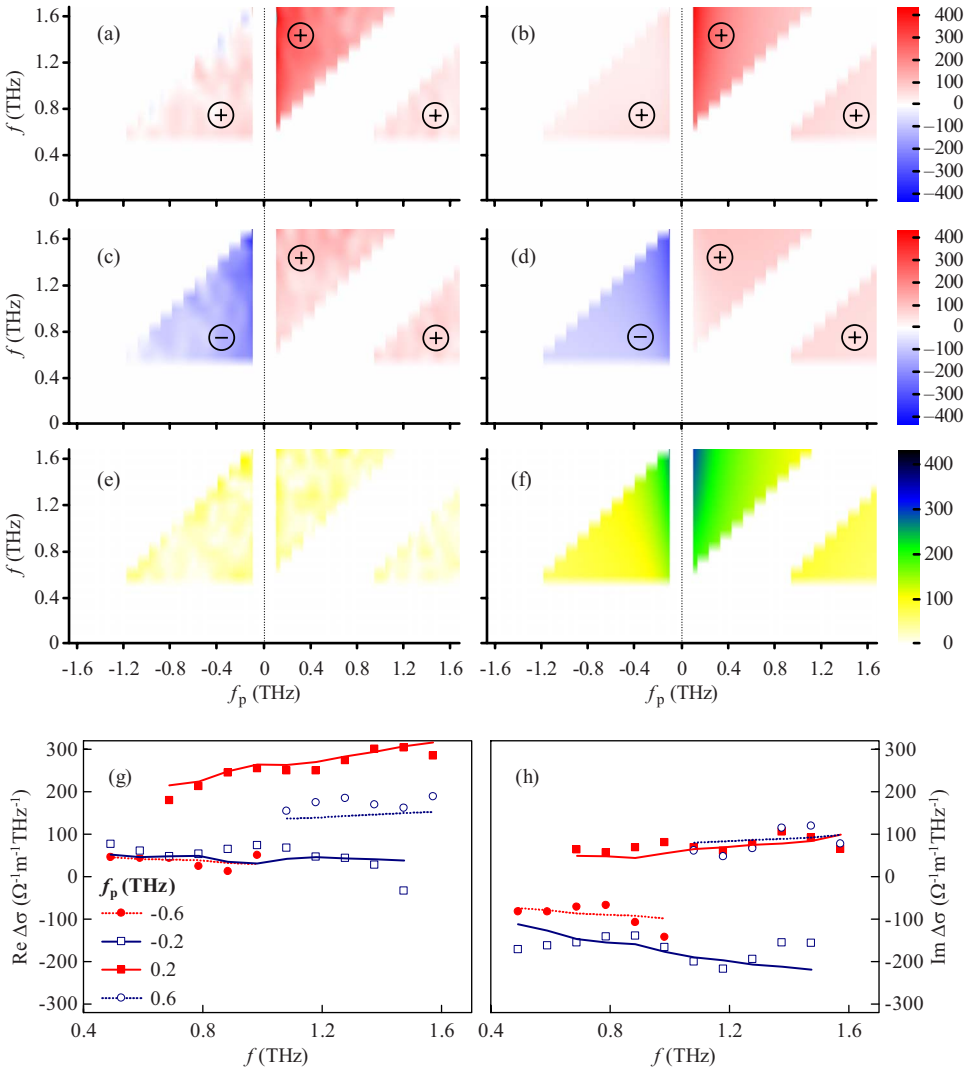

FIG. 3. (Color online) Spectrum (in Ω^{-1} m^{-1} THz^{-1}) of transient conductivity $\Delta\sigma$ in two-dimensional frequency domain. [(a) and (b)] Real part and [(c) and (d)] imaginary part of transient conductivity. [(a) and (c)] Measured data and [(b) and (d)] fit. (e) Amplitude of the residuals (amplitude of the difference between complex theoretical and measured conductivity). (f) Amplitude of the ultrafast component of the conductivity as obtained in the fit. The maximum of the color scale is common to all graphs. [(g) and (h)] Cuts of the real and imaginary parts of conductivity for various values of f_p. Symbols: experiment; lines: fit. The excitation wavelength for this kind of measurements was 800 nm.

of the slow relaxation which means that the conductivity in the low-frequency part of our THz spectrum would drop to zero as demonstrated in Fig. 2(c). This reasoning is not contradicted by the measurement of the temperature dependence of conductivity of P3HT.[18]

B. Ultrafast conductivity component

The measured transient conductivity spectra in the 2D frequency domain are plotted in Figs. 3(a) and 3(c). We find that the model expressed by Eq. (1)—describing the slow dynamics—must be complemented by two additional relaxation terms activated immediately after photoexcitation to obtain a good match with the measured spectra [Figs. 3(b) and 3(d)]. While the expression for time-dependent conductivity—or equivalently permittivity—spectrum of a relaxation is well known, the corresponding expression describing the ultrafast dynamics in the two-dimensional frequency domain is more complicated and we need to account for the decay of the carrier density

$$n(\tau_p) = n_0 \xi_0' \exp(-\tau_p/T_{\mathrm{trap}}') \tag{4}$$

and for a possible time dependence of the high-frequencies mobilities, e.g.,

$$\mu_j'(\tau_p) = \mu_{0,j}' \exp(-\tau_p/T_j'). \tag{5}$$

Here ξ_0' is the initial quantum yield, T_{trap}' is the decay time of carrier population (either due to trapping or recombination), $\mu_{0,j}'$ are the initial high-frequency mobilities, and T_j' are the mobility decay times (the primed quantities refer to the ultrafast component of conductivity). Since the relaxation is a specific case of the damped harmonic oscillator, we apply the general result derived in Ref. 32 [Eq. (49)] and calculate the relaxation response as a limit of an overdamped harmonic oscillator. In terms of Ref. 32 this means that the Green's function of the ground state vanishes (G_G=0) and that the relaxation time $\theta' \equiv \gamma_E/\omega_E^2$ is related to the eigenfrequency ω_E and damping γ_E in the excited state, where $\omega_E \gg 2\pi f$ and $\gamma_E \gg 2\pi f$. We can thus obtain for the ultrafast component of the conductivity

$$\Delta\sigma_{\mathrm{ultrafast}}(f,f_p) = n_0 e_0 \xi_0' \sum_{j=1}^{2} \left(\frac{\mu_{0,j}'}{\frac{1}{T_j'} + \frac{1}{T_{\mathrm{trap}}'} - 2\pi i f_p} \frac{2\pi i f - \frac{1}{T_j'} - \frac{1}{T_{\mathrm{trap}}'}}{2\pi i f - \frac{1}{T_j'} - \frac{1}{T_{\mathrm{trap}}'} - \frac{1}{\theta_j'}} \right). \tag{6}$$

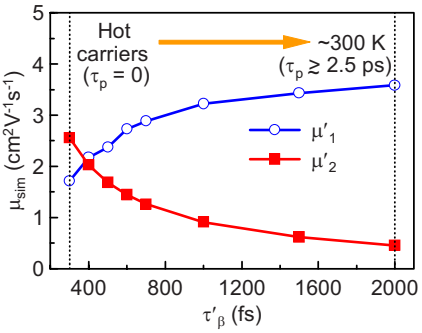

FIG. 4. (Color online) High-frequency mobilities as a function of τ'_β. The graph indicates the transition between the initial regime of hot carriers (effectively low potential barriers passed with the mean τ'_β=0.3 ps) and the quasiequilibrium state characterized by $\tau'_\beta=\tau_\beta$=1.9 ps.

Despite its certain complexity, the model of the ultrafast conductivity defined by Eq. (6) involves only six fitting parameters: $\xi'_0\mu'_{0,1}$, θ'_1, $1/T'_1+1/T'_{\mathrm{trap}}$, $\xi'_0\mu'_{0,2}$, θ'_2, and $1/T'_2+1/T'_{\mathrm{trap}}$. The following parameters provide the best match of the measured transient conductivity (Appendix B): $1/T'_{\mathrm{trap}}+1/T'_1=1/(860\ \mathrm{fs})$, $\theta'_1=115$ fs, and $\xi'_0\mu'_{0,1}=0.34\ \mathrm{cm^2\ V^{-1}\ s^{-1}}$; $1/T'_{\mathrm{trap}}+1/T'_2=1/(150\ \mathrm{fs})$, $\theta'_2\gtrsim 10$ ps, and $\xi'_0\mu'_{0,2}=0.57\ \mathrm{cm^2\ V^{-1}\ s^{-1}}$.

We assume that the ultrafast conductivity has the same physical origin as the slow component (i.e., origin of the primed parameters should be the same as that of the appropriate unprimed ones); the only difference consists in a higher excess energy of the nascent holes. The hot holes then pass more easily over the potential barriers. We find that the Monte Carlo calculation with the parameters inherited from modeling of the slow component (N_β and τ_{hop}) and with a shorter hopping-over-barrier time (τ'_β=0.3 ps) reproduces well the experimental results on the ultrafast scale and it allows to determine the initial high-frequency mobilities $\mu'_{0,1}=1.7\ \mathrm{cm^2\ V^{-1}\ s^{-1}}$ and $\mu'_{0,2}=2.7\ \mathrm{cm^2\ V^{-1}\ s^{-1}}$. The ratio of the measured conductivity and the calculated mobilities then provides an estimate of the initial yield $\xi'_0\sim 0.2$.

The dynamics of holes is controlled by the hopping-over-barrier time τ'_β. The finding that $\tau'_\beta<\tau_\beta$ indicates that hops over the barriers are more frequent at ultrashort times; hence the long-range (intersegment) transport is more efficient at the early transport stages ($\mu'_{0,2}>\mu_2$). We infer that the initial value τ'_β=0.3 ps progressively increases with the pump-probe delay τ_p as the carriers cool down to approach finally the value of τ_β=1.9 ps for $\tau_{\mathrm{p}}\gtrsim 2.5$ ps. The implications of this transition can be understood by the calculations of the mobility spectra with τ'_β varying between these limits. The resulting spectra can be fitted by a sum of two relaxations and the high-frequency mobilities corresponding to these relaxations are plotted in Fig. 4. We observe that μ'_2 is decreasing, i.e., the intersegment transport becomes less effective as the potential barriers become effectively higher (τ'_β grows). Conversely, μ'_1 increases, meaning that the intrasegment transport becomes dominant, i.e., that the carrier moves within one segment rather than between the segments. Note finally, that $\mu'_1+\mu'_2$ equals μ_{int} within our model: this can be understood given the fact that the high-frequency mobilities are insensitive to the presence of potential barriers.

Based on the results in Fig. 4, we can identify the meaning of the times T'_2 and T'_{trap}. The amplitude μ'_1 does not decay and for a qualitative view, we can consider that the mobility decay time T'_1 in Eq. (5) is infinite. The trapping time T'_{trap} then becomes approximately equal to the measured longer decay time: T'_{trap}=860 fs. In contrast, the amplitude μ'_2 decreases rather markedly as the carriers cool down and the shortest decay time of 150 fs then includes both T'_{trap} and T'_2. The time T'_2 is thus apparently the carrier cooling time, and we obtain $T'_2\approx 180$ fs.

The estimate of the initial photon-to-charge yield ξ'_0 is consistent with the external quantum efficiency of LBPP-1:PCBM-based solar cell ($\sim$10%).[22] However, we cannot state with certainty that the fraction of $1-\xi'_0$ of incident photons is not converted into separated charges. First of all, the estimate of the absolute value of ξ'_0 is inherently related to the mobility model developed in the paper, and it should be taken with a certain care. Moreover, the determination of the measured conductivity may be quite inaccurate due to the inhomogeneities of the investigated film. Finally, ξ'_0 does not account for separated charges possibly produced via intermediate states.[5] The yield of mobile charges at longer times is low [e.g., ξ(75 ps)$\sim$0.01] and it further decreases [Figs. 1(a) and 1(b)]. The process responsible for the low values of ξ is carrier trapping rather than carrier recombination, such a fast recombination would be incompatible with the external quantum efficiency of the LBPP-1:PCBM-based solar cells.[22] Moreover, transient absorption measurements of similar blends showed that there is no recombination on the time scale faster than 1 ns.[5] This means that after 1 ps the majority of holes is trapped: these do not contribute to the transient far-infrared spectra but they can still participate in the slow interchain transport and thus allow the solar cell operation. The observed slow (tens of ps) conductivity decay can be regarded as a slow approach toward equilibrium between populations of mobile and trapped holes.

Note that the assignment of the processes occurring on the subpicosecond time scale is to a large extent indirect and it relies on the observation of two dynamical components. The first one (860 fs) is related mainly to the population decay while the second one (150 fs) is related mainly to the mobility decay. Further confirmation of this assignment would require a use of other experimental methods. For example, time-resolved THz spectroscopy in multi-THz spectral region offers a better time resolution and also extra information about the transport mechanisms could be gained in a higher-frequency spectral range.[33]

IV. SUMMARY

We have used time-resolved THz spectroscopy to investigate microscopic transport of photogenerated carriers in a LBPP-1:PCBM blend and we have developed a simple theoretical model for understanding distinct stages of the transport. The microscopic transport is controlled by potential barriers on polymer chains which enclose segments of $\approx$4 repeat units. The holes are initially hot and they easily pass over the potential barriers—as a result, the initial hole mo-

bility is comparable to the polymer intrinsic mobility. Subsequently, the holes cool down at a fast rate of $(1/180\ \text{fs})^{-1}$, and they are trapped at an initial rate of $(1/860\ \text{fs})^{-1}$—these processes manifest themselves as a steep conductivity drop. At longer times, the conductivity decrease slows down considerably and it represents the equilibration of populations of mobile and trapped charge carriers.

ACKNOWLEDGMENTS

The studies were supported by the Swedish Energy Administration, by the Center of Organic Electronics funded by the Swedish Strategic Research Foundation, and by the Ministry of Education and Science Foundation of the Czech Republic (Projects No. LC-512, No. 202/06/0286, and No. 202/09/P099). H.N. also acknowledges the Guest Scholarship Programme of the Swedish Institute and L. Fekete for assistance with experiments.

APPENDIX A: ANALYSIS OF THE ULTRAFAST CONDUCTIVITY

In most of all-optical pump-probe experiments, the time lengths of the pumping and probing pulses are short compared to the time scale of the investigated processes. Optical pump-THz probe (OPTP) experiments provide a possibility to investigate ultrafast processes on a time scale shorter than the length of the probing THz pulse (~ 1 ps). However, in such a case, the spectral components of the broadband THz pulse mix with the spectral components of the ultrafast dynamical processes in the sample.[25,26] One needs to account for this phenomenon by using appropriate methods of the data analysis.[24,27,32,34–36]

In this paper, we used the recently developed approach based on a Fourier transformation into two-dimensional frequency domain.[24,26,27,32] This method applies to a weak photoinduced response, and its major advantage is that the transient photoconductivity $\Delta\sigma$ is calculated *directly* from the measured data using elementary mathematical operations only.

The total measured signal $\Delta E(\tau,\tau_p)$ contains both the ultrafast component $\Delta E_{\text{ultrafast}}(\tau,\tau_p)$ and the slow component $\Delta E_{\text{slow}}(\tau,\tau_p)$:

$$\Delta E(\tau,\tau_p) = \Delta E_{\text{ultrafast}}(\tau,\tau_p) + \Delta E_{\text{slow}}(\tau,\tau_p). \quad \text{(A1)}$$

While the ultrafast component vanishes for long pump-probe delays $[\Delta E_{\text{ultrafast}}(\tau,\tau_p)=0$ for $\tau_p \geq \tau_{p,\max}]$, the slow component persists for $\tau_p > \tau_{p,\max}$. This implies that a straightforward application of the Fourier transformation to $\Delta E(\tau,\tau_p)$ in the time-window $\tau_{p,\min} \leq \tau_p \leq \tau_{p,\max}$ would give rise to an artificial ringing in the spectra. To avoid the ringing, we extrapolated the slow component of the transient THz signal along τ_p:

$$\Delta E_{\text{slow}}(\tau,\tau_p) = \Delta E(\tau,\tau_{p,\max}) g(\tau_p) \quad \text{(A2)}$$

so that the Fourier transformation of $\Delta E(\tau,\tau_p)$ in the variable τ_p could be performed in an extended time window $\tau_{p,\min} \leq \tau_p \leq \tau_{p,\text{MAX}}$, where $\tau_{p,\text{MAX}} \gg \tau_{p,\max}$. The extrapolation function g describes the dynamical evolution of the slow component and it satisfies the following conditions: $g=0$ for $\tau_p < 0$ ps, $g=1$ for $\tau_p=\tau_{p,\max}$ and g decays to zero for $\tau_p \gg \tau_{p,\max}$. To emulate the real conditions, an exponential function g was selected with the time constant determined from the pump-probe scan. This procedure does not affect the ultrafast components (their response completely vanishes for $\tau_p > \tau_{p,\max}$), but it reproduces the slow components only approximately.

The extrapolation strategy must be correctly reflected in the modeling of the transient conductivity spectra. Analogically to Eq. (A1), the transient conductivity spectrum is decomposed into the ultrafast and the slow (extrapolated) component:

$$\Delta\sigma(f,f_p) = \Delta\sigma_{\text{ultrafast}}(f,f_p) + \Delta\sigma_{\text{slow}}(f,f_p). \quad \text{(A3)}$$

While an appropriate model for $\Delta\sigma_{\text{ultrafast}}(f,f_p)$ must be set up to learn about the ultrafast conductivity processes, the slow part of the conductivity $\Delta\sigma_{\text{slow}}(f,f_p)$ is unambiguously determined by the extrapolation procedure. In fact, the slow part of the transient conductivity in the two-dimensional frequency domain is calculated from the two-dimensional Fourier transformation of Eq. (A2) and it reads

$$\Delta\sigma_{\text{slow}}(f,f_p) = \Delta\sigma_{\text{slow}}(f,\tau_{p,\max}) g(f_p), \quad \text{(A4)}$$

where the spectrum of the transient conductivity at the end of the scan $\Delta\sigma(f,\tau_{p,\max})$ is calculated within the quasi-steady-state approximation in which one-dimensional Fourier transformations $\Delta\sigma(f,\tau_p)$ and $\Delta E(f,\tau_p)$ are mutually proportional.[23] The slow conductivity component being determined by Eq. (A4), the problem of fitting the entire conductivity of Eq. (A3) is reduced to the modeling of the ultrafast conductivity component $\Delta\sigma_{\text{ultrafast}}$ by Eq. (6).

APPENDIX B: FITTING PROCEDURE

From the properties of Fourier transformation it is clear that the transient conductivity of the slow component is localized in a close proximity of $f_p=0$ and that the spectrum of the ultrafast component is much flatter around the f_p axis and it decays slowly with f_p. To make the fitting procedure as insensitive as possible to the long-delay extrapolation procedure described in Appendix A, data with low f_p ($f_p < 0.1$ THz) were cutoff. As a result, the parameters obtained from the fitting procedure are insensitive to the profile of the extrapolation function g.

This treatment allowed a reliable determination of the six parameters describing the ultrafast components. The parameters are not much correlated among themselves: the parameters $\xi'_0\mu'_{0,1}$ and $\xi'_0\mu'_{0,2}$ define the amplitudes of the conductivity, the decay rates $1/T'_1+1/T'_{\text{trap}}$ and $1/T'_2+1/T'_{\text{trap}}$ determine the extent of the transient conductivity spectrum in the f_p direction and the relaxation times θ'_1 and θ'_2 control the conductivity shape in the f direction. The quality of the fit is demonstrated in Fig. 3(e). The residua are featureless which demonstrates the pertinence of the model and they are small compared to the amplitude of the ultrafast component of conductivity [Fig. 3(b)]. For clarity, one-dimensional spectral cuts for a few values of f_p are displayed in Figs. 3(c) and 3(d).

[1] C. J. Brabec, Sol. Energy Mater. Sol. Cells **83**, 273 (2004).
[2] I. G. Scheblykin, A. Yartsev, T. Pullerits, V. Gulbinas, and V. Sundström, J. Phys. Chem. B **111**, 6303 (2007).
[3] C. J. Brabec, G. Zerza, G. Cerullo, S. D. Silvestri, S. Luzzati, J. C. Hummelen, and S. Sariciftci, Chem. Phys. Lett. **340**, 232 (2001).
[4] F. Laquai, G. Wegner, and H. Bässler, Philos. Trans. R. Soc. London, Ser. A **365**, 1473 (2007).
[5] S. De, T. Pascher, M. Maiti, K. G. Jespersen, T. Kesti, F. Zhang, O. Inganäs, A. Yartsev, and V. Sundström, J. Am. Chem. Soc. **129**, 8466 (2007).
[6] D. Hertel, U. Scherf, and H. Bässler, Adv. Mater. **10**, 1119 (1998).
[7] T. J. Savenije, J. E. Kroeze, X. Yang, and J. Loos, Adv. Mater. **15**, 1260 (2005).
[8] V. I. Arkhipov, I. I. Fishchuk, A. Kadashchuk, and H. Bässler, *Photophysics of Molecular Materials* (Wiley-VCH Verlag, Weinheim, 2006), pp. 261–366.
[9] J. Cabanillas-Gonzalez, T. Virgili, A. Gambetta, G. Lanzani, T. D. Anthopoulos, and D. M. de Leeuw, Phys. Rev. Lett. **96**, 106601 (2006).
[10] F. A. Hegmann, O. Ostroverkhova, and D. G. Cooke, *Photophysics of Molecular Materials* (Wiley-VCH Verlag, Weinheim, 2006), pp. 367–428.
[11] C. A. Schmuttenmaer, Chem. Rev. (Washington, D.C.) **104**, 1759 (2004).
[12] H. Němec, P. Kužel, and V. Sundström, Phys. Rev. B **79**, 115309 (2009).
[13] E. Hendry, J. M. Schins, L. P. Candeias, L. D. A. Siebbeles, and M. Bonn, Phys. Rev. Lett. **92**, 196601 (2004).
[14] E. Hendry, M. Koeberg, J. M. Schins, H. K. Nienhuys, V. Sundström, L. D. A. Siebbeles, and M. Bonn, Phys. Rev. B **71**, 125201 (2005).
[15] E. Hendry, M. Koeberg, J. M. Schins, L. D. A. Siebbeles, and M. Bonn, Chem. Phys. Lett. **432**, 441 (2006).
[16] F. C. Grozema, P. T. van Duijnen, Y. A. Berlin, M. A. Ratner, and L. D. A. Siebbeles, J. Phys. Chem. B **106**, 7791 (2002).
[17] X. Ai, M. C. Beard, K. P. Knutsen, S. E. Shaheen, G. Rumbles, and R. J. Ellingson, J. Phys. Chem. B **110**, 25462 (2006).
[18] P. D. Cunningham and L. M. Hayden, J. Phys. Chem. C **112**, 7928 (2008).
[19] P. Parkinson, J. Lloyd-Hughes, M. B. Johnston, and L. M. Herz, Phys. Rev. B **78**, 115321 (2008).
[20] N. V. Smith, Phys. Rev. B **64**, 155106 (2001).
[21] H. Němec, H. K. Nienhuys, F. Zhang, O. Inganäs, A. Yartsev, and V. Sundström, J. Phys. Chem. C **112**, 6558 (2008).
[22] E. Perzon, F. Zhang, M. Andersson, W. Mammo, O. Inganäs, and M. R. Andersson, Adv. Mater. **19**, 3308 (2007).
[23] L. Fekete, P. Kužel, H. Němec, F. Kadlec, A. Dejneka, J. Stuchlík, and A. Fejfar, Phys. Rev. B **79**, 115306 (2009).
[24] P. Kužel, F. Kadlec, and H. Němec, J. Chem. Phys. **127**, 024506 (2007).
[25] J. T. Kindt and C. A. Schmuttenmaer, J. Chem. Phys. **110**, 8589 (1999).
[26] H. Němec, F. Kadlec, and P. Kužel, J. Chem. Phys. **117**, 8454 (2002).
[27] H. Němec, F. Kadlec, C. Kadlec, P. Kužel, and P. Jungwirth, J. Chem. Phys. **122**, 104504 (2005).
[28] A Debye relaxation is usually described in terms of its contribution to the susceptibility: $\Delta\chi_j(f)=X_j/(1-2\pi\mathrm{i}f\theta_j)$, where X_j denotes the dielectric strength of the relaxation. Equivalently, the dielectric relaxation can be expressed as a contribution to the conductivity via the well-known relation $\Delta\sigma_j(f)=-2\pi\mathrm{i}f\varepsilon_0\Delta\chi_j(f)$. The introduction of the mobility in Eq. (1) then reflects the fact that the conductivity is a product of charge density and (frequency-dependent) carrier mobility.
[29] P. Prins, F. C. Grozema, J. M. Schins, T. J. Savenije, S. Patil, U. Scherf, and L. D. A. Siebbeles, Phys. Rev. B **73**, 045204 (2006).
[30] H. Scher and M. Lax, Phys. Rev. B **7**, 4491 (1973).
[31] O. Hilt and L. D. A. Siebbeles, Chem. Phys. Lett. **269**, 257 (1997).
[32] H. Němec, F. Kadlec, S. Surendran, P. Kužel, and P. Jungwirth, J. Chem. Phys. **122**, 104503 (2005).
[33] R. Huber, C. Kübler, S. Tübel, A. Leitenstorfer, Q. T. Vu, H. Haug, F. Köhler, and M.-C. Amann, Phys. Rev. Lett. **94**, 027401 (2005).
[34] M. C. Beard and C. A. Schmuttenmaer, J. Chem. Phys. **114**, 2903 (2001).
[35] M. C. Beard, G. M. Turner, and C. A. Schmuttenmaer, J. Appl. Phys. **90**, 5915 (2001).
[36] H.-K. Nienhuys and V. Sundström, Phys. Rev. B **71**, 235110 (2005).